Materials Science & Engineering A 841 (2022) 142998

Contents lists available at ScienceDirect

Materials Science & Engineering A

journal homepage: www.elsevier.com/locate/msea

On the thermomechanical aging of LPBF alloy 718

Salomé Sanchez [a], G. Gaspard [b], C.J. Hyde [a,*], I.A. Ashcroft [a], G.A. Ravi [c], A.T. Clare [a]

[a] University of Nottingham, University Park, Nottingham, Nottinghamshire, NG7 2RD, United Kingdom
[b] École Polytechnique Fédérale de Lausanne, Lausanne, Switzerland
[c] Renishaw plc., New Mills, Wotton-under-Edge, Gloucestershire, GL12 8JR, United Kingdom

ARTICLE INFO

Keywords:
Laser powder bed fusion
Creep
Nickel alloy 718
Microscopy
Thermomechanical aging
Heat treatment

ABSTRACT

Heat treatment of products post additive manufacture are considered hugely important since the metallurgical condition post process is suboptimal. In the case of nickel-based superalloys, grain size, precipitate distribution and precipitate size are distinct from wrought equivalents. Appropriate heat treatment is required to ensure material performance. In this study, LPBF alloy 718, post-processed using a standard heat treatment, is explored under thermal and thermomechanical exposure conditions (with and without applied stress) to illustrate textural and microstructural evolution.

The results show the instability of the LPBF microstructure in terms of grain size, precipitate density, and crystallographic orientation, illustrating the need for an appropriate heat treatment in relation to future service conditions. During thermal exposure only, the instability of the LPBF alloy microstructure was evident as the texture increased with time before decreasing and almost disappearing at the time of fracture. This contrasts with wrought alloy whose texture increases throughout creep testing and reaches a maximum at the time of fracture. An ideal microstructure for improved creep performance was identified and includes large equiaxed grains, elimination of texture, dissolution of Laves and δ phase and the precipitation of small carbides and γ'' precipitates. Recommendations on how to heat treat LPBF alloy 718 to reach this microstructure are given. Overall, this work showed that LPBF components may become more performant than wrought and conventional equivalents.

1. Introduction

Resistance to creep, which is a deformation process that occurs at high temperatures over extended periods of time, is crucial for components operating under elevated temperatures and stresses with long service life, such as aero engine turbine blades. Components' ability to withstand high loads and temperatures is key to engine efficiency [1] and to operate under these conditions, components are usually manufactured from nickel-based superalloys which have excellent mechanical integrity at high temperatures. This family of alloys has the highest temperature and strength combination of cast and wrought superalloys at elevated temperatures, which makes them ideal for critical engineering applications. Alloy 718 is a nickel-based superalloy with particularly good creep properties. This alloy's main phase is the γ-phase (NiCr) and the main strengthening phases, beneficial to creep properties, include γ′ and γ'', face centred cubic $Ni_3(Al, Ti)$ and body centred cubic Ni_3Nb, respectively [2]. At high temperatures, γ'' phase transforms to δ phase, which has the same composition as γ'' (Ni_3Nb) but with an orthorhombic packing. The δ phase has been stated as both beneficial [3] and detrimental [2] to creep properties. Other detrimental phases include the Laves, carbides and topologically closed packed phases. All these phases can modify the alloy's behaviour by their composition, morphology and location [2]. Alloy 718 is also the main nickel-based superalloy employed in Additive Manufacturing (AM) research [4], due to its superior Laser Powder Bed Fusion (LPBF) manufacturability [5]. Like other AM processes, LPBF is capable of fabricating complex designs - which can result in better efficiency and performance - and has the potential to save money, time, and material, compared to traditional manufacturing methods, [4]. These advantages make LPBF attractive to industries where high value components with low production volumes components are required [4].

A review of the powder bed fusion of nickel-based superalloys showed that the most studied mechanical properties were tensile and hardness properties, whereas fatigue and creep, have been researched much less [4]. From the creep studies to date, some found that LPBF alloy 718 performed more poorly than wrought [6], forged [7] or cast

* Corresponding author.
E-mail address: christopher.hyde@nottingham.ac.uk (C.J. Hyde).

https://doi.org/10.1016/j.msea.2022.142998
Received 11 January 2022; Received in revised form 11 March 2022; Accepted 14 March 2022
Available online 16 March 2022

[8] alloy 718, whereas others found that LPBF material outperformed their wrought counterparts, for both tensile [8] and compressive [9] creep tests. Multiple studies also investigated the effects of LPBF process parameters - such as build orientation [10] and scan strategies [11], multi-laser strategies [12] - and the effects of post-processing [13] and heat treatment [14] on the creep properties of LPBF alloy 718. One of the key observations is that the heat treatments commonly employed for LPBF alloy 718 are not ideal, having been designed for conventional materials. There is therefore a need to deepen the understanding of LPBF microstructure and its effect on mechanical properties to be able to develop a suitable heat treatment for LPBF materials that can further increase mechanical performance. In this study, this will be investigated for the creep properties of alloy 718 to address the research gap in terms of number of studies on creep.

To do this, the LPBF creep mechanisms must be understood first to determine the necessary microstructural features required to improve the creep rate and life of the material. A previous study compared the microstructure of LPBF alloy 718 before and after creep [7]. However, there is still a need to observe and understand the evolution of the LPBF 718 microstructure during creep. Xu et al. developed a novel staged creep testing method where 2-bar creep specimens were creep tested and non-destructively analysed at various times during the creep test using X-ray Computed Tomography (XCT) to identify the location of defects in the specimens, which were then used to successfully predict and identify the position of fracture [15]. This method provided a better understanding of the creep behaviour of LPBF alloy 718 and the key role that process induced porosity and defects play during creep. However, the creep tests in this study were shorter than 14h [15], which means that creep damage may not have had time to develop. The authors of the present work found that with suitable process parameters, a LPBF alloy 718 specimen obtained a similar creep rate and outperformed its wrought counterpart by 24% in terms of creep life, lasting over 500h at 650 °C and 600 MPa load [16]. Typical creep damage (micro-ovoid coalescence) was clearly visible after failure of these LPBF specimens, which provides confidence that creep actually occurred [16]. It would therefore be beneficial to better understand the creep mechanisms occurring and the microstructural evolution of a LPBF specimens which outperformed wrought alloy 718 during creep.

Overall, a review of the literature showed that there is a lack of understanding of the effects of LPBF microstructure on creep. Thus, there is a necessity to have a better understanding of the behaviour of LPBF alloy 718 during creep to determine the necessary microstructural features required to improve the creep properties and inform heat treatment design. Therefore, for the first time, interrupted creep tests will be performed on a LPBF alloy 718 specimen which outperforms wrought alloy 718 in the aim to understand the microstructural evolution of LPBF alloy 718 during creep and to provide the research community with a recommendation of the microstructure and heat treatment required to further improve LPBF creep performance.

2. Experimental methods

To observe defect and microstructural evolution during creep, interrupted creep tests were conducted. Both LPBF and wrought alloy 718 were investigated to understand the effects of their distinct microstructures on creep mechanisms and identify the features resulting in better creep properties.

This paper builds upon previous work from the authors [16] and hence, some of the previously generated creep data and microscopy images are used here. The images used will be clearly referenced in the captions. The LPBF specimen with the best creep rate and creep life from that study, a heat treated alloy 718 specimen built at 90° build orientation with the Meander scan strategy (90° Meander HT), was selected and compared to wrought alloy 718 of the same composition, supplier and batch. The reader is directed to the authors' paper to obtain the details on the specimens - powder composition, LPBF process parameters, heat treatment, machining methods – and microstructural analysis methods and data processing. In addition to the quantifiers described in the other paper, grains' aspect ratios were obtained using Electron Back Scatter Diffraction (EBSD) scans processed with the HKL Channel 5 software by Oxford Instruments (Abingdon, UK).

The interrupted creep tests used the same machine, procedures and loading conditions (650 °C and 600 MPa) as in the previous work [16]. From the creep curves obtained in that work, the secondary and tertiary creep regions were identified, and the time of mid-secondary and mid-tertiary creep were pinpointed for both the LPBF and wrought specimen. The breakpoints are illustrated in Fig. 1. The times of these breakpoints are different for LPBF and wrought alloy 718 and can be found in the table under the graph (calculated from Ref. [16]).

At each breakpoint, the specimens were removed from the creep test furnace and prepared for microstructural analysis. The specimens were not returned to the creep testing machine as they were destructively prepared for Scanning Electron Microscopy (SEM) and EBSD analysis. Hence, different specimens were used to characterise the material microstructure at each breakpoint.

To isolate the contribution of load and temperature during creep, LPBF specimens were also thermally exposed at 650 °C in the creep furnace with no load and interrupted at the same breakpoints before being analysed by SEM and EBSD. For this experiment, the specimens were mounted in the creep testing machine to ensure the thermal histories of the unloaded samples were identical to those subjected to creep testing. The images presented in this paper are all oriented with respect to the creep test loading direction (LD) for easy comparison, from the point of view of the mechanical test. Where relevant, the build direction (BD) of the specimens is also indicated.

3. Results

This section will present the creep curves and associated microstructure evolution of wrought and LPBF alloy 718 during creep and thermal exposure.

3.1. Creep response

Fig. 2 presents the creep strain-time curves for the various creep tests performed with the wrought alloy 718 and LPBF 90° Meander HT specimen. Fig. 2a and b are the creep curves previously obtained by the authors [16], which were used to identify the breakpoints of the wrought alloy 718 and 90° Meander HT specimens, respectively.

Table 1 presents the results of the creep tests for the wrought and LPBF alloy 718. Similar minimum creep rates were obtained for the wrought and LPBF specimens and the latter had a longer creep life. The

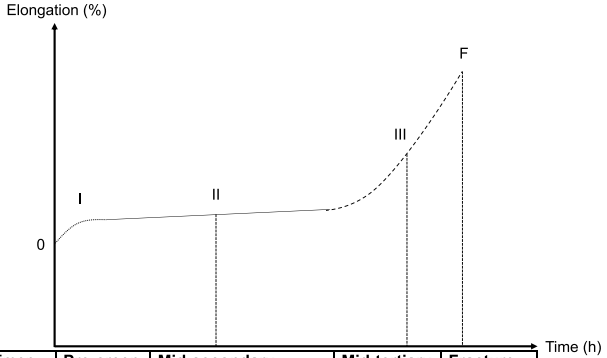

Specimen	Pre-creep	Mid-secondary	Mid-tertiary	Fracture
LPBF	0h	121h	430h	507h
Wrought	0h	123h	331h	409h

Fig. 1. Graphical representation of the breakpoints for staged and interrupted creep tests.

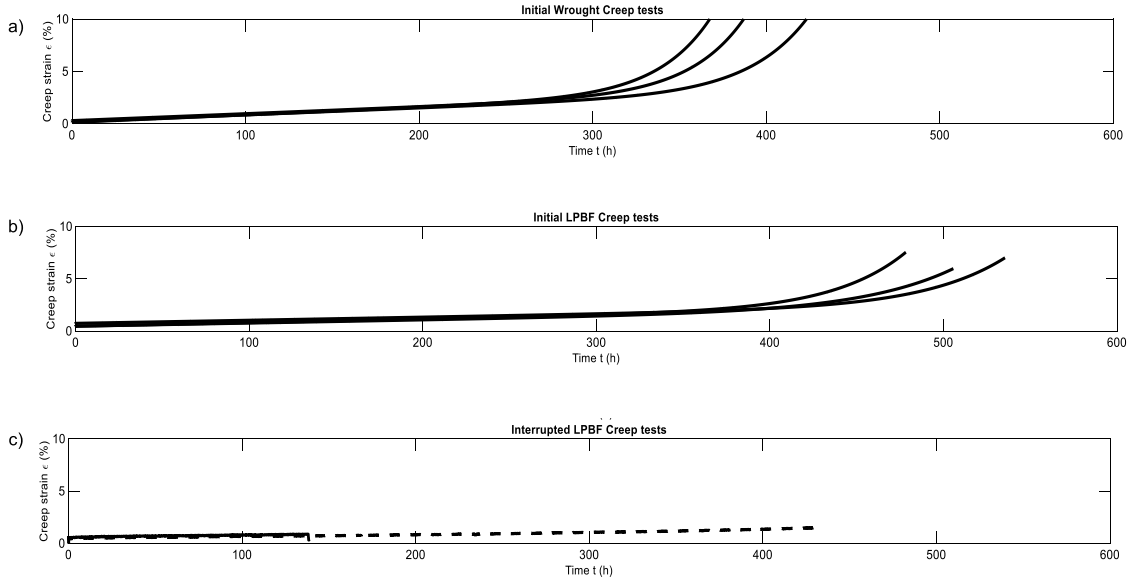

Fig. 2. Creep curves for the different types of creep tests. a) Initial creep tests of wrought alloy 718 used to identify the breakpoints. b) Initial creep tests of 90° Meander HT specimen used to identify the breakpoints of the LPBF alloy 718. c) Interrupted creep tests for mid-secondary and mid-tertiary breakpoints of LPBF alloy 718.

Table 1
Creep properties for the wrought and LPBF alloy 718.

Specimen	Minimum creep rate (10^{-3} h^{-1})	Creep life (h)	Elongation at fracture (%)
Wrought	2.47	409 ± 8	29.3 ± 0.1
LPBF	2.46	507 ± 13	7.5 ± 0.5

time in tertiary creep of wrought alloy 718 also has a more exponential aspect and higher elongation at fracture (which was cut off at 10% in Fig. 2a to allow better visualisation of the LPBF curves). The low scatter between the LPBF alloy 718 specimens' individual curves can be observed, which brings confidence that the different specimens used during the interrupted creep tests are a fair representation of the 90° Meander HT specimens.

Fig. 2c shows the LPBF alloy 718 interrupted creep tests, where two different specimens were interrupted within the mid-secondary and mid-tertiary regions, at 121h and 430h, respectively. The specimens from these creep tests were used for microstructural analysis and to investigate the evolution of the microstructure during creep for the wrought and LPBF specimens.

3.2. Microstructural evolution

The evolution of the microstructure during creep for wrought and LPBF alloy 718 will be presented first, followed by the evolution of the LPBF microstructure during thermal exposure only, without load.

Illustrative examples of texture evolution for the different types of specimens are shown in Fig. 3. Table 2 quantifies and summarises the material descriptors, such as density, grain size and precipitate density present at various stages of the creep life for the specimens.

3.2.1. Wrought alloy 718 during creep

Fig. 4 shows the microstructure evolution for the wrought alloy 718 during creep. Some key observations from, which are also supported by Table 2 and Fig. 3, include:

- Before creep, the grains are small and equiaxed (Table 2 and Fig. 4a), with an average grain size of 82 ± 2.45 μm^2.
- As creep time increases, the grains of wrought alloy 718 have a 41.5% reduction in area (Fig. 4c, Table 2 and Fig. 3a'''').
- The grain morphology seems to change from equiaxed to elongated in the loading direction (Fig. 3a''), although the average aspect ratio is relatively unchanging, with a 12% difference between the pre-creep and fracture microstructures (Fig. 4 and Table 2).
- There is an increase in <111> texture in the loading direction as creep progressed with a maximum texture at the time of fracture (Fig. 3a-a'''').

The wrought alloy 718 also had δ-precipitates clearly visible at the grain boundaries as thin needle-shaped precipitates throughout the creep test (Fig. 4a'-d'). Carbides were also present in the material as large globular precipitates at the grain boundaries (Fig. 4a'-c'). These were identified from their Nb-rich content compared to the matrix [17] and their preferred precipitation at the grain boundaries [18], which is typical for alloy 718 [19]. As time progresses during the creep test, the number of carbides seems to increase (Fig. 4b and c), which is consistent with the data presented in Table 2 that shows an augmentation of pre-cipitate density as creep progresses. Carbide cracking can also be seen (Fig. 4b' and c') and the voids initiated by the carbides are also responsible for the decreasing density of the material, as shown in Table 2. The small microvoids initiated by δ-precipitates on the grain boundaries (Fig. 4d'), also contribute to the accumulated creep damage and decreasing density.

Overall, the wrought alloy 718 microstructure is isotropic with car-bides and δ-precipitates present before creep. These observations will be used as reference and comparison for the LPBF alloy 718 specimen.

3.2.2. LPBF alloy 718 during creep

Fig. 5 shows the microstructure of the 90° Meander HT specimen at the various stages during testing. There were pores and defects present both in the grains and at grain boundaries, as shown in the SEM images (Fig. 5a). As the creep test progresses, microvoids initiate (Fig. 5b') and coalesce (Fig. 5c') until cracks form (Fig. 5d and d'), which is a typical creep damage evolution mechanism. As shown in Fig. 5, most of the microvoids are smaller than 2 μm. It is also noticeable that most microvoids initiate at the grain boundaries near δ-precipitates [16], which have previously been shown to cause crack initiation [20]. As well as δ-precipitates, the LPBF material also had small and globular

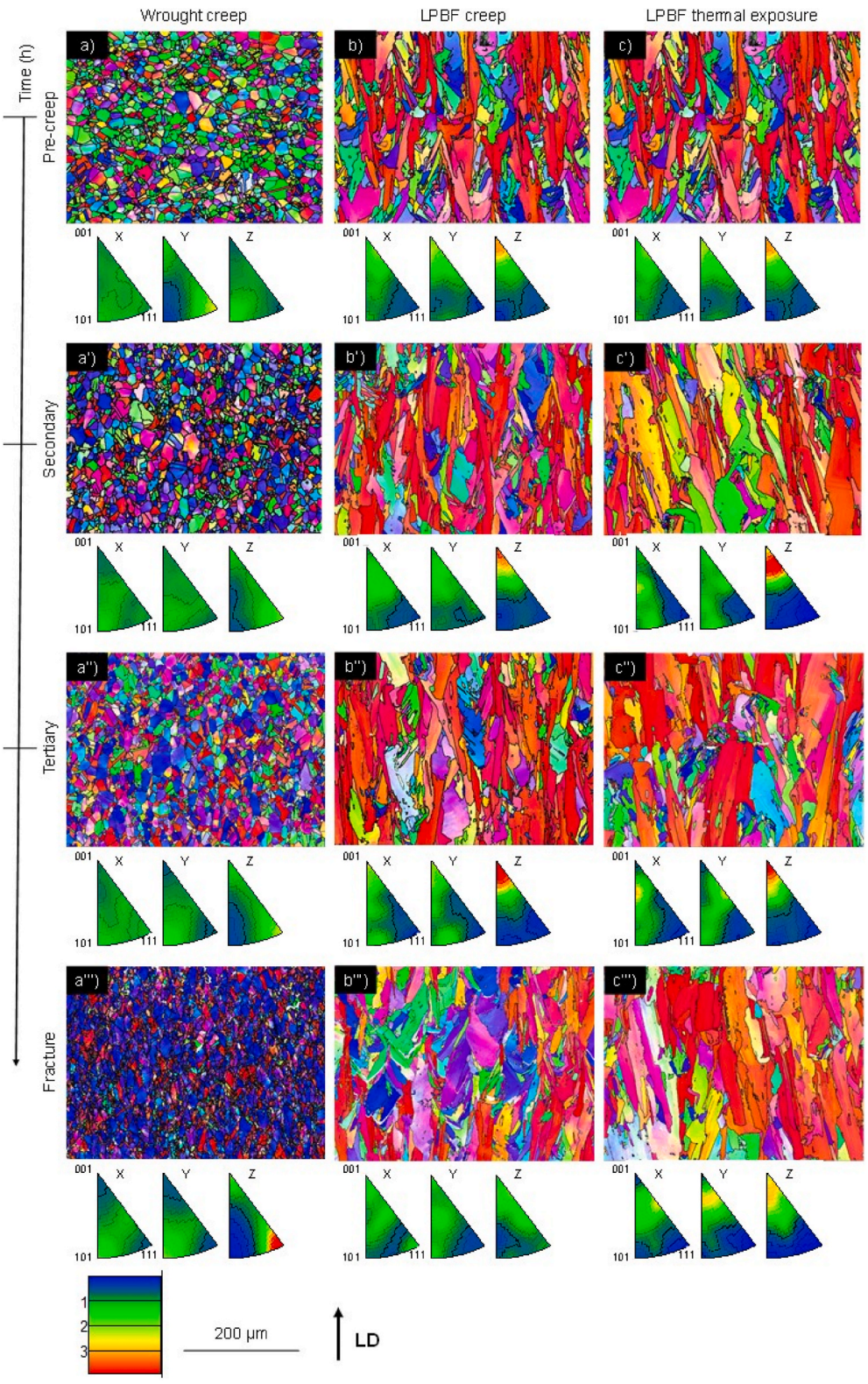

Fig. 3. EBSD maps and Inverse pole figures showing the evolution of texture with time for the different specimens. a-a''') Wrought alloy 718 during creep showing an increase in texture along the loading direction as creep progresses. b-b''') LPBF alloy 718 during creep where the texture increases in the loading direction as creep progresses before disappearing at fracture. c-c''') LPBF alloy 718 during thermal exposure showing an increase then decrease in texture, highlighting the instability of the microstructure. The Z direction corresponds to the loading direction for all specimens and to the build direction as well for the LPBF specimens. (Images a, b and c were taken from the authors' previous work [16]).

Laves phase and carbides (Fig. 5a'). As only SEM was used to identify precipitates, γ'' could not be visualised. However, these precipitates should be present nonetheless.

The grain size of the LPBF specimen increased by a factor of 2.7 during creep (Table 2 and Fig. 3b and b'''). The grains also became more elongated during creep strain in the direction of loading, which could have also increased their area (Fig. 5a, c), although this is not clearly visible in SEM and EBSD images. However, the aspect ratio has a 16% increase from pre-creep to fracture, which confirms the elongation of the grains during creep (Table 2). The texture of the LPBF specimen also varied during creep, as shown in Fig. 3b-b'''. Before creep, there is a <001> texture parallel to the build direction, then, the texture increases as creep progresses, in a similar fashion to wrought alloy 718, but interestingly, the texture disappears after fracture (Fig. 3b'''). This

Table 2
Quantification of the evolution of the microstructure during for wrought and LPBF alloy 718 during creep and for the LPBF alloy 718 during thermal exposure only. The pre-creep and 0h data for each specimen was taken from Ref. [16].

Specimen	Average specimen density (± *0.15 %Area)*	Average precipitate (carbide, laves, δ) density *(± 0.15 %Area)*	Average grain size *(μm²)*	Average grain aspect ratio
Wrought Pre-creep	100	2.97	82 ± 2	2.53 ± 0.03
Wrought Mid-Secondary	99.9	2.79	103 ± 3	2.26 ± 0.03
Wrought Mid-Tertiary	99.9	3.22	70 ± 2	2.49 ± 0.03
Wrought Fracture	99.8	4.12	48 ± 1	2.26 ± 0.02
LPBF Pre-creep	99.9	0.22	129 ± 13	3.08 ± 0.08
LPBF Mid-Secondary	95.0	0.48	179 ± 16	3.36 ± 0.07
LPBF Mid-Tertiary	88.5	0.59	222 ± 24	3.86 ± 0.11
LPBF Fracture	86.0	0.61	346 ± 35	3.58 ± 0.10
LPBF thermal exposure 0h	99.9	0.22	129 ± 13	3.08 ± 0.08
LPBF thermal exposure 121h	99.88	0.82	360 ± 63	4.19 ± 0.16
LPBF thermal exposure 430h	99.83	1.27	246 ± 45	3.36 ± 0.08
LPBF thermal exposure 505h	98.37	1.47	362 ± 61	3.98 ± 0.12

phenomenon will be explained in section 4.2.

The changes in microstructure observed in the LPBF specimens are due to the load and temperature applied during the creep test. To differentiate the effects of load and temperature, the microstructure evolution of the thermally aged specimens without mechanical load will now be discussed.

3.2.3. LPBF alloy 718 during thermal exposure only

Fig. 6 shows the microstructure evolution of the thermally exposed LPBF alloy 718 specimens (to compare with the pre-creep microstructure, the reader is directed to Fig. 5a and a'). After 121h, the microstructure of the thermally exposed specimen seems similar to that of pre-creep (Fig. 6a), with elongated columnar grains parallel to the build direction and δ-precipitates, carbides and Laves phase on the grain boundaries (Fig. 6a').

The main difference observed is the more important presence of large pores (Fig. 6a''). These pores seem to thermally expand with time, becoming larger (Fig. 6b'' and c). This is particularly noticeable in Fig. 6c''. This increase in pore size is the main reason for the decreasing density observed in Table 2. Both spherical and irregular pores expanded.

From Table 2, the grain size of the thermally exposed specimen increases by a factor of 2.8 from pre-exposure to 505h, which is similar to the creep tested specimen. However, the grains first observe a strong increase after 121h before the grain size lowers at 430h and increases again by 505h. This unsteady variation will be discussed further in the next section of the paper. The morphology of the grains remains elongated and columnar but also seem to be more defined (Fig. 6a and c). The aspect ratio of the grains increases by 29% with time (Table 2), confirming the more columnar aspect of the grains after 505h. The number of precipitates increases with time during the thermal exposure, by a factor of 6.7 (Table 2), although this is not clearly visible in the SEM images (Fig. 6a'-c').

The thermally exposed specimen had a <001> texture parallel to the build direction before the test and the texture increases until 121h. Then, it decreases after 430h before becoming weak at the time of fracture (Fig. 3c-c'''). The variation in crystallographic orientation of the thermally exposed specimen indicates that the heat treatment used for the LPBF specimen is not appropriate for subsequent exposure of parts at elevated temperature for extended periods in service as this results in an unstable microstructure.

4. Discussion

The results show the differences in microstructural behaviour during creep of LPBF and wrought alloy 718. These highlighted the unstable nature of the LPBF microstructure, further indicating the need for an appropriate heat treatment to improve creep performance. The separate effects of the creep loading conditions and thermal exposure of LPBF alloy 718 were also observed. These results will now be discussed.

4.1. Evolution of porosity

Fig. 7 shows the evolution of part density with time for the creep tested and thermally exposed LPBF specimens. Some key observations are:

- The reduction in density in the thermally exposed LPBF specimen corresponds to pore expansion.
- The density steadily decreases in the creep tested LPBF specimen, at a faster rate than the thermally exposed equivalent.
- For the creep tested LPBF specimen, the slightly larger reduction in density corresponds to creep damage, in the form of microvoids and cracks, which ultimately gave rise to fracture. It is likely that pore expansion also occurs in the creep tested specimens, but to a lesser degree.

The pores are inbuilt during the LPBF process. Spherical pores come from gas entrapment and irregular pores form as a result of poor inter track/layer fusion or pores resulting from keyhole closure [21]. Porosity has always been a determining factor for creep performance and has recently been shown to be the most influential factor affecting the creep rate, more so than other LPBF process factors such as build orientation and scan strategy [22]. Another interrupted creep study also found that the main crack initiation points were pores [23], more specifically irregular pores [24]. The expansion of pores here is due to the thermal exposure and to the opening of the pores caused by the creep load. From the above arguments, it is obvious that porosity in LPBF specimens must be reduced to improve and assure creep performance.

4.2. Evolution of texture

Fig. 3a-a''' showed the evolution of texture in the wrought alloy 718 during creep. It was observed that the texture increases throughout the creep life, being strongest at the time of fracture (Fig. 3a'''). This increase in texture was also observed by another study before and after creep for forged alloy 718 [7]. The study proposes that the increase in texture may be due to grain rotation which occurs due to stress accommodation in the build material. Therefore, it is proposed that the strain of the equiaxed grains in the loading direction, which causes them to rotate slightly and have a slight change in aspect ratio, is the reason for the increase in texture.

Similarly to wrought alloy 718, the LPBF creep tested specimens had

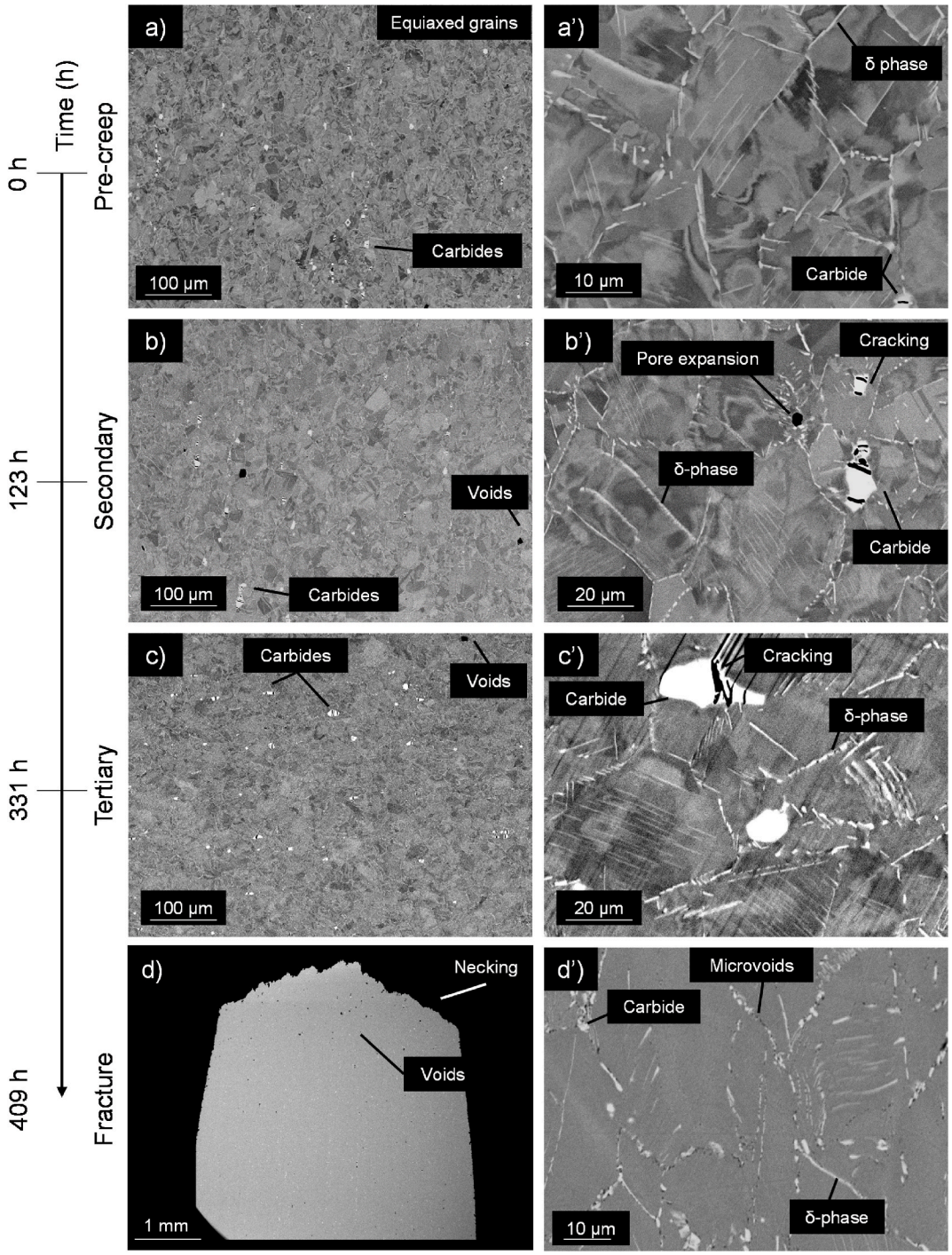

Fig. 4. SEM images of the microstructural evolution of wrought alloy 718 during creep. a-a') Pre-creep microstructure (a' taken from Ref. [16]). b-b') Microstructure in the secondary region, after 123h of creep. c-c') Microstructure in the tertiary region, after 331h of creep test. d-d') Microstructure after fracture from Ref. [16]. This shows the increase in the number of carbides and carbide cracking.

an increasing texture with life as an effect of the creep load (Fig. 3b-b''). This is different from what was observed in another study where there was almost no texture difference between before and after creep in LPBF alloy 718 [7].

In comparison, the thermally exposed only specimens had an increase of texture until at least 121h before the texture started to reduce and almost disappear around the time of fracture (Fig. 3c-c'''). Hence, it can be inferred that the point at which the texture starts to reduce happens between 121h and 430h when exposed at 650 °C. Since the texture has not fully disappeared by 505h (Fig. 3c'''), it can be inferred that more time is needed at 650 °C to fully remove the texture. Huang et al. also found that a minimum amount of time is required at a given solution temperature to result in similar microstructures and mechanical properties than longer hold times and inversely, that for a fixed amount of time, a higher solution temperature would result in similar microstructures [25].

Compared to the creep tested LPBF specimen, there is more texture at the time of fracture in the thermally exposed specimen (Fig. 3c''') than in the creep tested specimen (Fig. 3b'''), whereas it was expected that the strongest texture would be present at the time of fracture in the creep

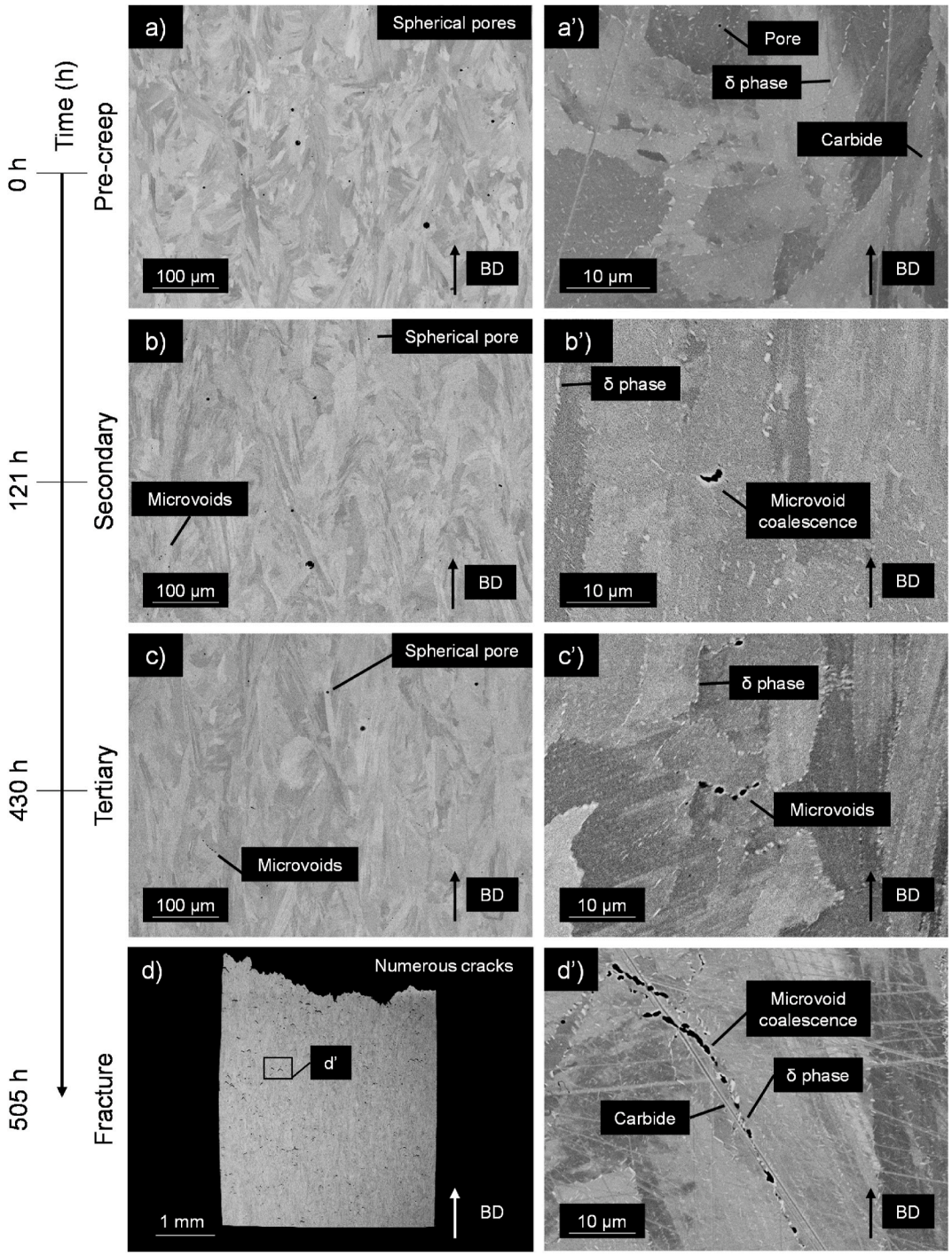

Fig. 5. SEM images of the microstructural evolution of LPBF alloy 718 during creep. a-a') Pre-creep microstructure from Ref. [16]. b-b') microstructure in the secondary region, after 121h of creep. c-c') microstructure in the tertiary region, after 430h of creep test. d-d') microstructure after fracture (505h), from Ref. [16]. This shows microvoid initiation at δ-phase on the grain boundaries and their coalescence as creep progresses.

tested LPBF specimen. This was caused by a prolonged exposure at 650 °C for 35h in the furnace after the creep test, which was conducted to confirm the effects of thermal exposure on the texture of this alloy. This explains the lack of texture due to the creep load at fracture and shows that in this work on LPBF alloy 718, the texture disappeared at some point between 505h and 540h when thermally exposed at 650 °C.

Additionally, the variation in texture observed in the thermally exposed LPBF specimen shows the instability of the LPBF microstructure and hence, demonstrates that the conventional heat treatment used is not suitable for the microstructure of the LPBF alloy 718. This is to be expected since the heat treatment used was design for wrought alloy 718, which has a different condition of supply microstructure when compared to the LPBF alloy 718.

From Fig. 3, the <001> texture observed in the creep tested specimen was parallel to the build direction which also coincided with the loading direction. In the thermally exposed specimens, the texture was also mostly present in the build direction, even after 430h. Hence, both the build direction and the loading direction, influence the direction of texture in LPBF material. The build direction dictates the original orientation of texture, while the loading direction influences the

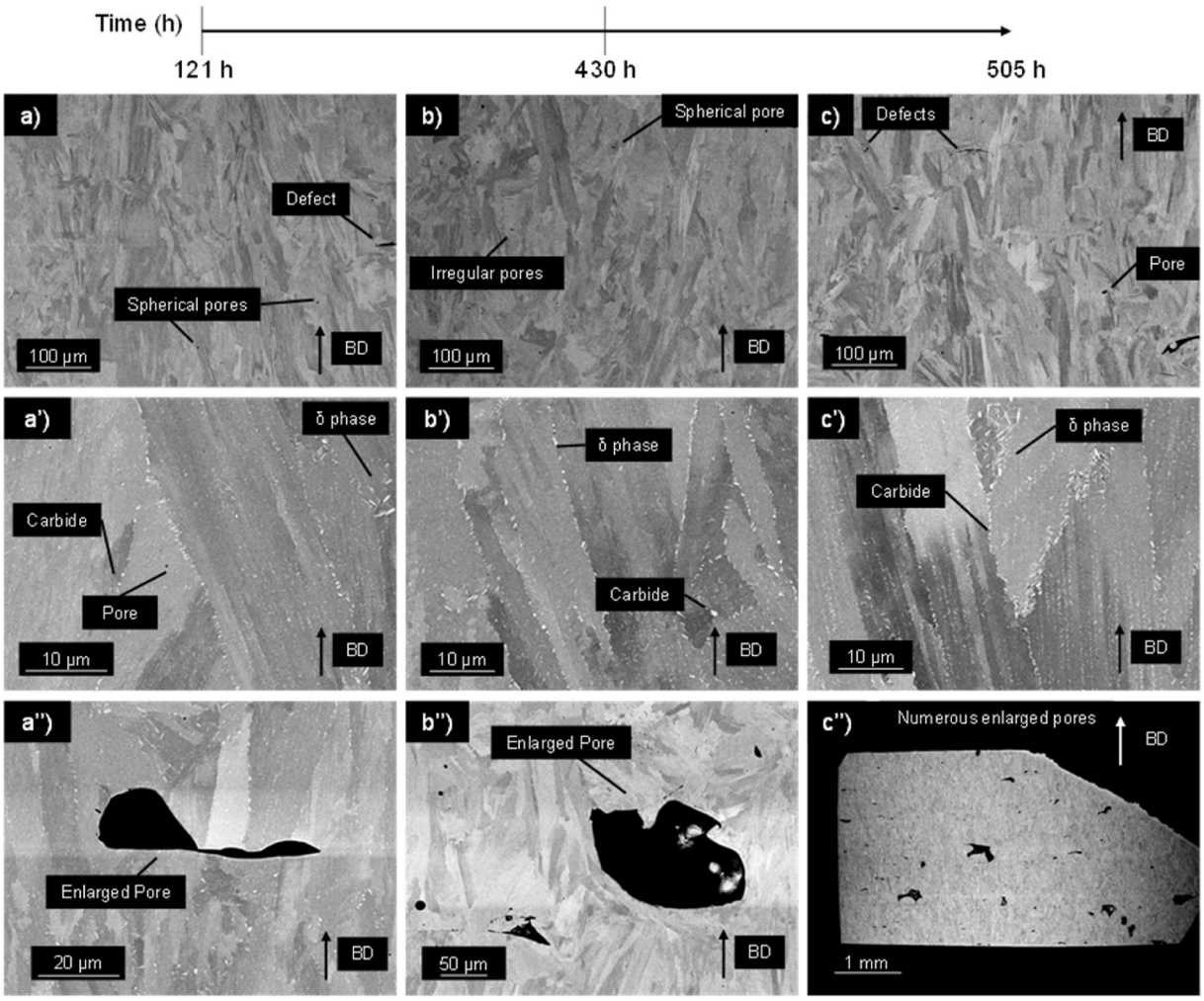

Fig. 6. SEM images of the microstructural evolution of LPBF alloy 718 during creep. a-a'') microstructure after 121h of thermal exposure. b-b'') Microstructure after 430h of thermal exposure. c-c'') Microstructure after 505h of thermal exposure. This shows the expansion of pores in the specimen and the increase in grain size.

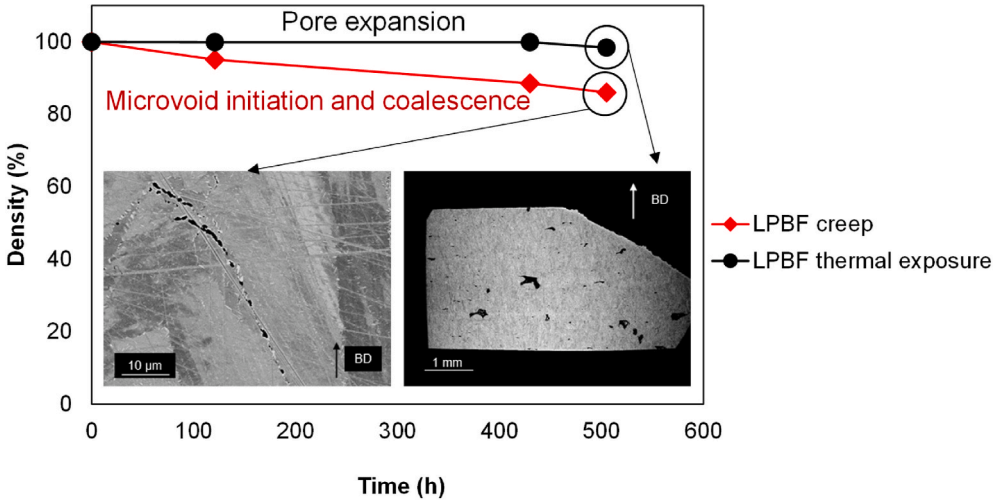

Fig. 7. Evolution of part density for the LPBF alloy 718 specimens during creep testing and thermal exposure. This figure was based on the data available in Table 2. This shows the increase in porosity in both specimens due to pore enlargement (thermal exposure) and creep damage (creep tested specimen).

orientation of texture which develops during creep. The texture in the build direction is explained by the preferential grain growth in <001> which is promoted by the elongated columnar structure of the LPBF grains. This in turn is caused by the dominant direction of heat flux on cooling which drives solidification and crystallisation [26]. The loading direction impacts the orientation of texture development during creep

due to elongation of the grains, as shown by the increasing aspect ratio in the LPBF specimen (Table 2). However, because the loading direction and build direction of the LPBF specimens are coincident in this work, it is difficult to evaluate how the different effects of the build and loading directions on the texture evolution interact, hence, a similar investigation with samples at other build orientations would be worthy of future work. It is hypothesised that when the texture of the specimen is off-axis with the load, the texture would be reduced through creep, which, if correct, could provide a useful tool for engineering a desired texture.

It is important to understand and control texture as the crystallographic orientation affects the mechanical performance of materials. For alloy 718, Bean et al. found that the grain texture alignment with the tensile axis reduced yield strength but enhanced ductility [27], while Ni et al. also suggested that the differences in ductility and strength in LPBF specimens was in part caused by the <100> fibre texture in specimens, which was thought to result in higher strength perpendicular to the build direction [28]. The texture of the 90° specimens was in line with the tensile axis (loading direction) during creep, which could be the reason for the higher elongation at fracture, compared to other build orientations (e.g. 0° and 45°) [16]. Moreover, the higher strength perpendicular to the build direction as described by Ni et al. likely proved beneficial to the 90° specimens as this strengthened their failure plane. Another study also suggested that a strong crystallographic texture can trigger texture-related strengthening mechanisms [29]. Therefore, it is recommended to either remove texture or to engineer it such that it is optimised for creep life within in the blank geometry of service components.

4.3. Evolution of grain size and morphology

Fig. 8 shows the evolution of grain size with time for the different types of specimens. The grain size of wrought alloy 718 is observed to decrease with creep time (Fig. 8). This is probably caused by dynamic recrystallisation, which is the nucleation and growth of new grains during deformation processes, as opposed to heat treatments. In dynamic recrystallisation, new grains form under strain by consuming atoms from pre-existing grains. Rettberg et al. observed localised dynamic recrystallisation during creep of two nickel-based superalloys, primarily near voids and clusters of carbides [30]. The small variation in grain size (Fig. 8) is an indicator of the stability of the wrought microstructure as well as its very low standard variation (which cannot be observed in Fig. 8 due to its small size).

In contrast, the evolution of LPBF grain size clearly shows the instability of the LPBF microstructure which can be attributed to the inappropriate heat treatment. For the LPBF specimen, the thermal exposure resulted in a significant increase in grain size before recrystallisation and grain growth occurred (Fig. 8). Thermodynamic effects [31] and residual stresses [32] are believed to drive grain growth and recrystallisation at high temperatures. The texture may have driven the rapid grain growth until 121h (Fig. 3c') and when the texture started to reduce (Fig. 3c''), recrystallisation may have started to take place. The creep tested LPBF specimen's grain growth occurred at a slower rate due to the load effect during creep which may have caused it to grow in a more controlled manner (similar to wrought alloy 718).

A previous study found that a longer solution time led to an increase in grain size in forged alloy 718, which was attributed to the dissolution of δ-phase [33]. Here, the final grain size (354 ± 48 μm on average) may be the stabilised size for LPBF alloy 718 since it was achieved after similar periods of time, regardless of load applied, by both types of LPBF specimens during creep or thermal exposure only.

It is well known that larger grains are beneficial for creep performance [34], as a low grain boundary density is favourable for high creep resistance. This is because fewer grain boundaries means that there are fewer sites for microvoid initiation and propagation. The wrought specimens had significantly smaller grains, by at least 57%, than the LPBF specimen while its creep life and creep rate were shorter and similar, respectively, than the LPBF specimen. There are various creep models which explain the effect of grain size on the creep rate. Garofalo's model states that grain boundaries are both a source and a barrier to dislocation motion [35]. Berger et al. found that a modified Garofalo equation was able to model the creep behaviour of Waspaloy [36]. However, grain size cannot be the only determinant factor for the superior creep strength of LPBF alloy 718 [37].

Grain morphology and aspect ratio may also have a part to play in determining changes during creep. The thermally exposed LPBF specimens retained and even emphasized their columnar morphology, as was observed from the 29% increase in their aspect ratio (Table 2). A previous study found that the columnar grain structure was retained and that there was no increase in grain size during solution treating at 980 °C [38], which was the solution temperature used in the present work. The creep tested LPBF specimen also retained a mainly columnar morphology as creep progressed, achieving its highest aspect ratio at the time of mid-tertiary creep (Table 2 and Fig. 3c''). Although the aspect ratio was slightly less at the time of fracture (Table 2) and the grains appeared slightly less columnar (Fig. 3), compared to the time in tertiary. This could be explained by the prolonged thermal exposure after fracture, during which the grains became more equiaxed, reducing their directionality and hence, reducing the texture. This indicates that an

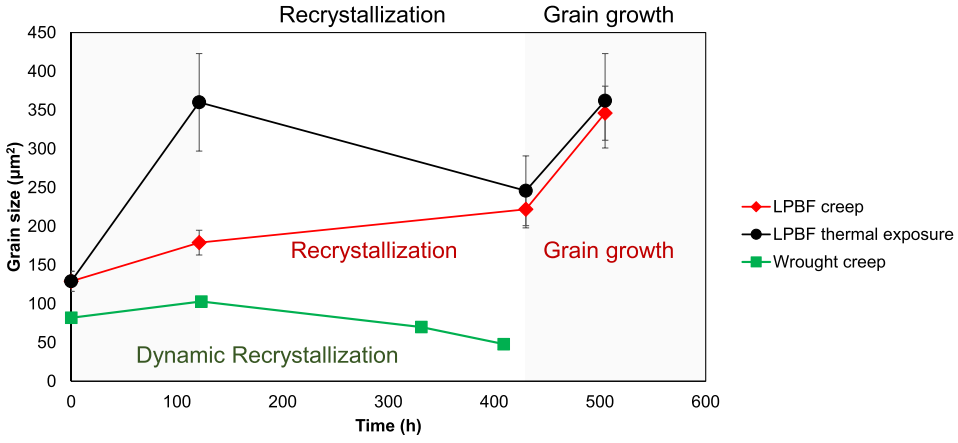

Fig. 8. Evolution of the grain size for the wrought alloy 718 during creep and the LPBF alloy 718 specimens during creep and thermal exposure. This figure was based off the data available in Table 2. This shows the dynamic recrystallisation of grains in the wrought alloy 718 during creep and the instability of the grains and their growth in both LPBF specimens.

appropriate heat treatment could make the grains more equiaxed and reduce texture in LPBF specimens.

The columnar aspect of the LPBF grains affected the creep response of the material. A previous study observed that large columnar grain structures make it difficult for the grains to pivot during creep deformation, which means that local stress concentrations are not alleviated, which leads to poor creep life and elongation at fracture [7]. Whereas for the wrought specimen, the small equiaxed grains were able to rotate during deformation, which releases accumulated local stress concentration and leads to a lower creep rate and higher elongation at fracture. Hence, the equiaxed nature of the wrought grains were beneficial to creep performance despite their small size, particularly in terms of elongation at fracture. The orientation of the columnar grains also affects the ductility of the part, with higher ductility observed when the columnar grains are parallel to the loading direction [39]. This may be one of the reasons that this LPBF specimen had a higher elongation at fracture than some 0° and 45° counterparts, as shown in other studies [12]. On the other hand, having columnar grains parallel to the loading direction is the basis of directionally solidified alloys, which are often used in turbine blades for their high creep resistance [34]. This feature may further explain why the present LPBF specimen outperformed its wrought equivalent.

From this analysis, large grains are beneficial to creep, as well as either equiaxed grains or columnar grains in line with the loading direction. However, microstructural design in this case must be undertaken with the upmost regard for the loading case in question which may not be uniaxial as reported here.

4.4. Evolution of precipitates

Fig. 9 shows the evolution of precipitate density with time for the different specimens. This shows that in all specimens the number of precipitate particles increased with time, but to different degrees.

The loss of mechanical performance can be attributed to the coarsening or decrease of strengthening precipitates [40]. More specifically, creep life is said to be attributed to the type, amount, and distribution of γ′, γ′′ and δ phase [41]. Other studies have also observed that the dissolution or transformation of γ′′ precipitates to δ cause a decrease in mechanical properties [42]. The precipitates observed here include δ-phase, carbides and Laves. The γ′′ were too small to be observed with SEM and are not included in the average precipitate density but should be present, nonetheless. This discussion will focus on the evolution of carbides, δ phase and γ′′. For background on the role of δ phase on the creep behaviour of LPBF alloy 718, the readers are directed to the authors' previous work [16].

The precipitates in the wrought material increased by 39% between the beginning of the creep test and the time of fracture (Fig. 9). This is probably due to the formation and growth of carbides. $M_{23}C_6$ carbides form at lower temperatures on the grain boundaries and have a block or granular appearance as reported elsewhere [43]. A study which performed interrupted creep tests at 950 °C and 210 MPa on a nickel-based superalloy found that carbides parallel to the loading direction cracked at regular intervals after 100h [23]. Cracked carbides were also visible in the present work after 123h (Fig. 4 b'). This cracking can serve as crack initiation and propagation points during creep and accelerate damage in tertiary creep [23]. This may explain why, despite having a similar creep rate to the LPBF alloy 718, the wrought material had a shorter creep life, mainly caused by having a rapid and short tertiary creep (Fig. 2a and b).

Despite these negative effects, other studies have found that small, coherent, closely packed needle-shaped $M_{23}C_6$ on the grain boundaries can improve rupture life [23]. These types of carbides may be present in the LPBF alloy 718 (Fig. 5a') as they were not as large and globular as the ones found in their wrought equivalent. These smaller carbides may contribute to pinning the grain boundaries, and acting as a strengthener [44].

Some studies observed that heat treatments (ageing at 650 °C for 168h [19], solution treating at 980 °C for 1h [45]) and HIP treatments [46] did not affect the formation or growth of carbides, probably because the temperatures were too low. Indeed, high homogenisation temperatures were shown to result in larger carbide size [47], which is said to be stable up to 1200 °C [48]. A study found that after 200h at 1200 °C, the carbide size did not change, indicating an equilibrium had been reached [49]. Therefore, it is unlikely that the increase in precipitate density in the wrought alloy 718 was from an increase in carbide size. Elemental composition and solidification rates control carbide morphology. For example, by increasing the cooling rates, more discrete, blocky-type MC carbides are formed [50]. Slower cooling rates were shown to result in larger carbides [46], which could explain the size of the carbides in the wrought specimen since it was furnace cooled at the various breakpoints during the interrupted creep testing. The increase in precipitate density in the wrought material is more likely to be an increase in carbide number. A qualitative inspection of Fig. 4a–c clearly shows an increase in the number of large globular precipitates, identified as carbides, which correlates to the increase in precipitates observed in Fig. 9. In the LPBF specimens, although some carbides were present, most of the precipitates on the grain boundaries seemed to be δ phase.

Both LPBF specimens had small needle shaped δ phase at the grain boundaries with the occasional small blocky/globular carbides (Figs. 5 and 6). The formation temperature of the δ phase is between 650 °C and 980 °C [51] and precipitation strengthening of the γ'/γ" phases occur at

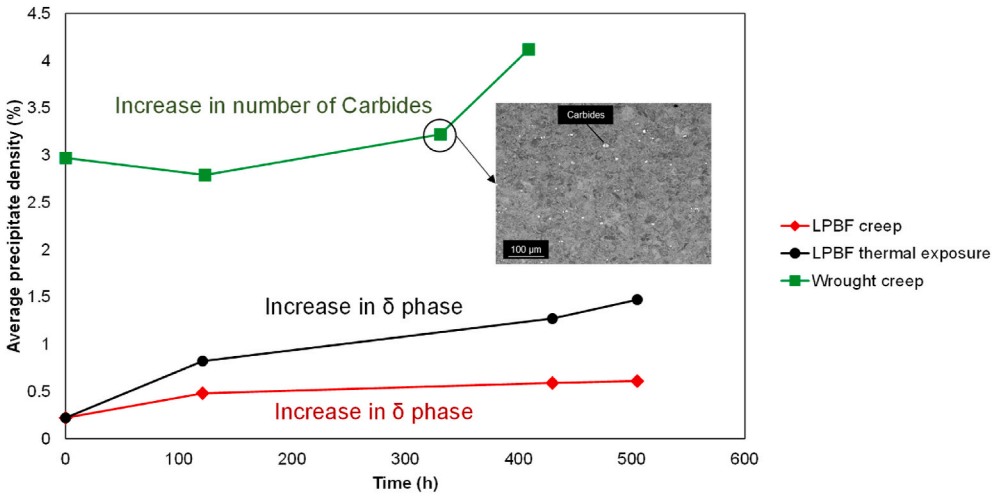

Fig. 9. Evolution of the average precipitate density in the wrought alloy 718 during creep and the LPBF alloy 718 specimens during creep and thermal exposure. This figure was based off the data obtained from SEM image analysis and is available in Table 2. This shows the increase in precipitate density in the wrought alloy, caused by an increasing number of carbides. It also shows the smaller increase in precipitate density between the creep tested and thermally exposed LPBF alloy 718 specimens.

600 °C–750 °C [29]. The heat treatment employed in this work (980 °C/1 h/Ga quench, 720 °C/8h/Furnace cooling to 620 °C/8 h/Ga quench) means that both δ phase and γ'/γ'' would have been precipitated, although γ'' precipitates are not visible here. γ'' precipitates are the main strengthening phase in alloy 718 and affect creep performance. For example, the creep deformation rate is controlled by the rate of γ'' coarsening [52] and creep damage increases as the amount of γ'' decreases [7]. In forged material, γ'' size and shape remain stable during creep whereas in LPBF material, γ'' size increases and transforms into δ phase [53]. Hence, the amount of γ'' precipitates decreases when the amount of δ-precipitates increases, as they both require Nb [41]. So, in theory, the less there is of δ-precipitates, the more there is of γ'' precipitates which results in better creep performance. Indeed, some studies found that without δ-precipitates, creep life is doubled and elongation at fracture quintupled [54]. Another study found that when the amount of δ phase was reduced to a minimum, larger grain sizes were obtained, which are beneficial to creep performance [33]. Conversely, too little δ phase resulted in crack initiation, just enough δ phase could stabilise the microstructure, improve strength, and prevent grain growth, while too much δ phase decreased the strength and plasticity of the material [55].

From Fig. 9, it can be seen that the thermally exposed specimens exhibited a higher increase in precipitate density than their creep tested counterpart. This may be another sign of the instability of the microstructure. Xu et al. found that there was an unstable transformation of γ'' to δ phase during creep of LPBF alloy 718 potentially driven by residual stresses [7]. In a study on alloy 718, δ-precipitates were mainly stable but slightly coarsened when exposed for 10,000 h at 650 °C and γ'' showed very little coarsening [48]. This shows that with the right temperature and hold time, the precipitates can be stabilised.

The difference in precipitate density between the thermally exposed and creep tested specimen (Fig. 9) also indicates that the load applied during creep affects the precipitate density. A study observed that the

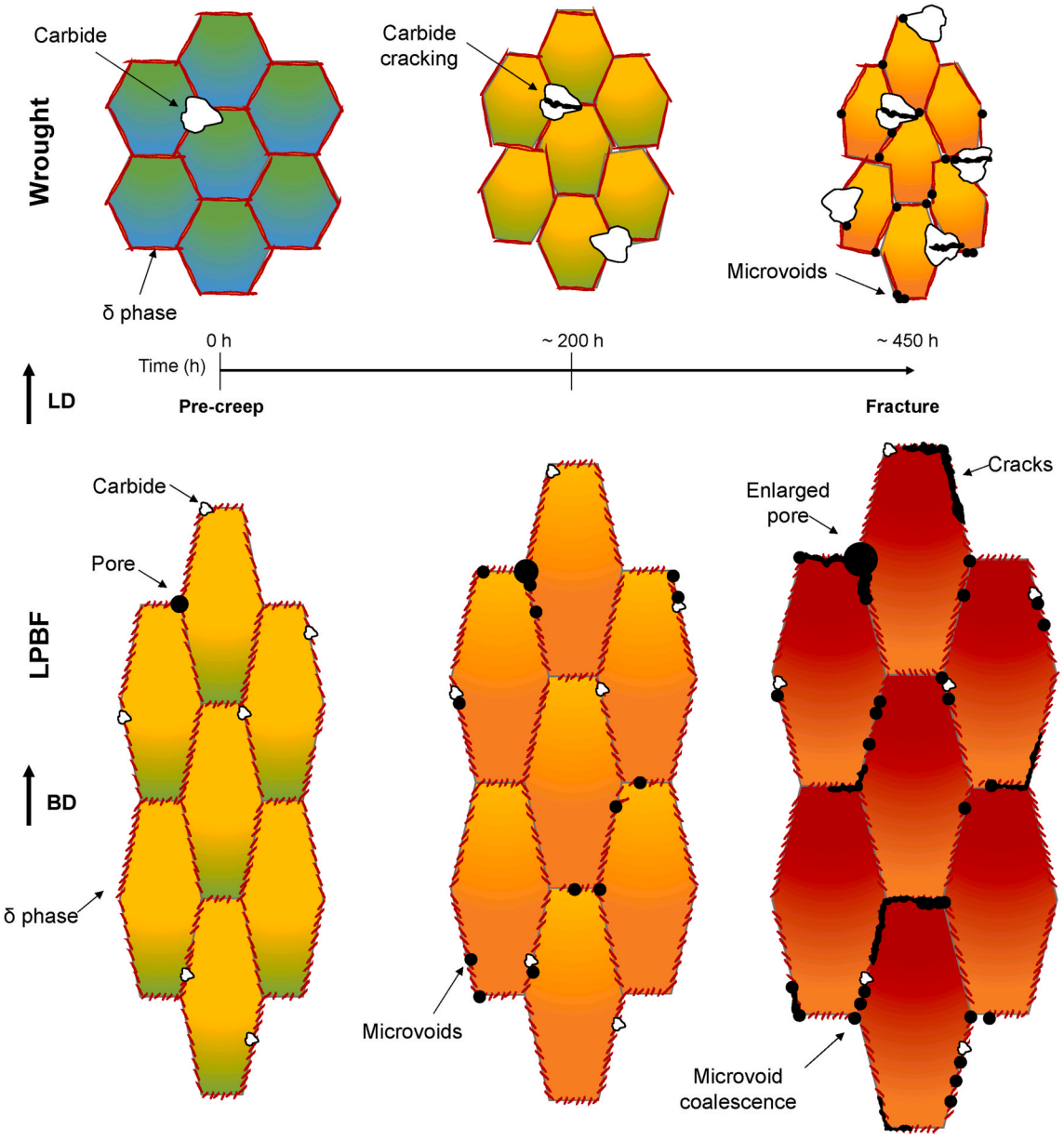

Fig. 10. Schematic representation of the microstructural evolution of wrought and LPBF alloy 718 during creep. The microstructures are drawn in relative scales, highlighting the bigger grain size of LPBF alloy 718, compared to its wrought equivalent. The colour in the figure symbolises the texture in the specimen, with warmer colours representing stronger textures. The time stamps given are approximately ±50h. (For interpretation of the references to colour in this figure legend, the reader is referred to the Web version of this article.)

total amount of δ phase increased with strain [56], which affects the precipitation kinetics [57]. This was observed previously for wrought alloy 718 [58]. However, despite the overall increase in δ-precipitates, the number of needle shaped δ-precipitates decreased while blocky ones increased [56]. However, neither the increase in precipitate density or morphology was observed in the LPBF creep specimens (Figs. 5 and 6) here. This may be because δ-precipitates form on grain boundaries and that in the LPBF alloy 718 specimens, grain size increases, which results in less grain boundaries and hence, less opportunities for δ-phase to nucleate. Therefore, the lower increase in precipitate density (corresponding to δ phase, carbides or Laves) observed in Fig. 9 for the LPBF creep tested material could be one of the reasons for the longer creep life observed in the LPBF alloy 718 compared to the wrought specimen as this would allow more precipitation of γ'' and less sites for crack initiation.

Overall, the precipitation of the strengthening γ'' phase is the most important for creep performance along with the dissolution of the detrimental phases. Small discrete carbides also seem to be useful for improving creep performance while large globular ones need to be avoided. This can be achieved through precision heat treatment.

4.5. Strategies for improved creep performance

From the above observations, it is possible to understand the microstructural evolution during creep of both wrought and LPBF alloy 718, which is schematically represented in Fig. 10 (In Fig. 10, the grain size for the wrought and LPBF alloy 718 is drawn to relative scale - highlighting the bigger grain size of LPBF alloy 718, compared to its wrought equivalent. The colours of the grains in Fig. 10 symbolise the texture in the specimen, with warmer colours representing stronger textures. Finally, the morphology of the grains was represented as regular polygons for illustrative purposes only.).

In the wrought alloy 718 during creep:

- The grains become smaller, have a slight change in aspect ratio and rotate to accommodate stresses
- The texture increases in the loading direction during creep.
- The number of carbides increases and carbide cracking occurs perpendicular to the loading direction.
- The carbides, the carbide cracks and the δ-precipitates serve as microvoid initiation points which result in accelerated creep damage in the tertiary creep region, compared to LPBF alloy 718, which explains their shorter creep life.

In the LPBF alloy 718 during creep:

- The grains become larger, more elongated and columnar in shape and do not rotate.
- The texture increases in the loading direction during creep, but the LPBF specimen starts with a much stronger texture than its wrought equivalent.
- Pores expand.
- Microvoids initiate at the δ phase and small carbides on the grain boundaries then coalesce and form cracks on the grain boundaries perpendicular to the loading direction, leading to fracture.

The Standard Specification for Additive Manufacturing Nickel Alloy (UNS N07718) with Powder Bed Fusion [59] provides recommendations for thermal processing of LPBF nickel-based superalloys. For heat treatments, the UNS N07718 points practitioners to the AMS2774 standard for heat treatment of wrought nickel alloy and cobalt alloy parts [60]. This standard provides different heat treatment options based on the geometry and type of nickel-based superalloy. However, all these heat treatments were designed for conventionally manufactured materials and not for LPBF material, which has a very different starting microstructure than the wrought, cast or forged equivalents. Therefore, the current heat treatments in use are potentially suboptimal, resulting in an unstable microstructure with a lack of strengthening phase precipitation, partial dissolution of detrimental phases and semi-recrystallised grains, as was observed throughout this work. This clearly indicates the need to develop LPBF specific heat treatments, to obtain superior mechanical properties. From the above discussion, useful features for high creep performance were identified as:

- Low porosity
- Large equiaxed grains
- No texture
- Precipitation of γ'' and small discrete carbides on the grain boundaries
- Dissolution of Laves and δ phases

To reduce the porosity, HIP treatments could be used as they have been shown to cause densification [61] and close cracks [62]. HIP has also been shown to reduce anisotropy [63] and improve fatigue resistance [64] and other mechanical properties [65]. However, a reduction in porosity can also be achieved through LPBF process parameter optimisation. For example, the scan strategy [21] and the volumetric energy density [66] have been shown to affect porosity. By controlling porosity through LPBF process optimisation instead of using HIP, saves time and resources and further increases the appeal of using LPBF as a suitable manufacturing method for critical engineering components.

While recent studies have found that the distribution, size, and morphology of Laves phase can be advantageous to mechanical properties [67–69], the general consensus is still that Laves phase is detrimental to creep properties and should be dissolved. A previous study found that a solution treatment at 1100 °C for 7h of LPBF alloy 718 resulted in the dissolution of Laves and δ phase [70]. Controlling the amount of δ phase is key to tailoring the mechanical properties of LPBF materials [9]. Dissolving the δ phase and Laves phase is desirable for maximising strength as it allows more γ'' precipitation [71]. The δ phase has a solvus temperature of 1010 °C and can precipitate between 650 °C and 980 °C [51] preferentially at grain boundaries, and less preferentially near MC carbides [72]. The amount of δ phase is proportional to the ageing time [54] and the size of the δ-precipitates increases consistently with decreasing cooling rate [72].

The high number of large globular carbides were identified as one of the key factors why wrought alloy 718 had a shorter creep life than the LPBF specimen, as they accelerate damage in tertiary creep. However, closely packed needle-shaped $M_{23}C_6$ precipitates at the grain boundaries were shown to improve rupture life [50] and intergranular fracture has been achieved with a near continuous carbide layer on grain boundaries [19]. By increasing the cooling rates, more discrete, blocky-type MC carbides can be formed [50] which could be beneficial to LPBF processed materials, by increasing their elongation at fracture.

Although some studies argue that phase precipitation is not necessary to strengthen AM materials if dislocation cells are retained [73], promoting strengthening precipitates, such as γ'' should increase creep strength. Indeed, higher compressive creep strength after solution HT at 1000 °C can be attributed to higher precipitation of γ'' since there is less Nb depletion from δ and Laves phases [9]. Precipitation strengthening of the γ'/γ'' phases occurs around 600–750 °C [29]. In LPBF alloy 718, γ'' precipitation occurred during double ageing typically performed at 720 °C and 620 °C [61,74]. Although double ageing is the norm for γ'' precipitation, the temperatures at which these are typically performed result in δ phase precipitation as well, which should be avoided for optimal creep performance. This is because in solution and ageing treatment, Nb segregation only partially dissolves, and this results in δ precipitates at the grain boundaries and in inter-dendritic regions [41]. Therefore, double ageing may not be recommended for creep performance.

While the columnar grain morphology and strong texture parallel to the loading direction present in LPBF materials strengthen the specimen,

this is dependent on the build direction. Indeed, other build orientations (e.g. 0° and 45°) have performed less well in terms of creep rate and life, which is partly due to their grain orientation and texture at an angle from the loading direction [16]. To eliminate texture, a more equiaxed microstructure is key [75]. Therefore, eliminating the columnar aspect of the grains would allow parts manufactured at different build orientations to have similar mechanical performances. Tucho et al. found that a solution treatment at 1100 °C for 7h of LPBF alloy 718 resulted in grain coarsening which suggests the completion of recrystallisation [70].

Taking the above requirements into account, a recrystallisation heat treatment developed by Kouraytem et al., consisting of a 625 °C/h ramp up rate, a 1h dwell time at 1250 °C, and a 625 °C/h ramp down rate [76], should produce the desired features. Indeed, this heat treatment resulted in a 3-fold increase in grain size, a change in grain morphology from columnar to equiaxed, a reduction in the <001> texture, the dissolution of Laves phase and of the majority of the δ phase (only 1 in 30 grains had small intergranular δ-precipitates), as well as the precipitation of nano γ′ and γ'' precipitates [76]. This heat treatment seems to tick all of the boxes for the suggested microstructure required for improved creep performance, although this has not been verified here. If larger grains are required, the dwell time could be increased. For an increase in γ'' precipitation the ramp down rate could be reduced to 300 °C/h maximum, or a single aging step at 620 °C could be undertaken, which should not trigger the precipitation of δ phase.

Finally, although heat treatments can contribute to microstructure engineering [77], research should also focus on obtaining the desired microstructure through the LPBF process alone. This would greatly improve the appeal of AM technologies and allow more microstructural engineering design freedoms.

5. Conclusions

This work explored the evolution of LPBF alloy 718 during creep to provide suggestions on how to improve creep performance. Building on previous work [16], interrupted creep tests were designed and wrought and LPBF alloy 718 were analysed at breakpoints in secondary and tertiary creep regions. Thermal exposure of LPBF specimens at the same breakpoints were also conducted to understand the individual effects of load and temperature on the creep performance. Key findings are summarised below:

- The increase in grain size and precipitate density in the LPBF alloy 718 is a sign of unstable microstructure caused by an unsuitable heat treatment designed for wrought alloy 718.
- The load applied during creep causes grains to rotate and have a slight change in aspect ratio in wrought and LPBF alloy 718, resulting in an increase in crystallographic texture with time.
- Thermal exposure at 650 °C for over 540h was shown to eliminate texture in LPBF alloy 718.
- The decrease in grain size in the wrought alloy 718 during creep is thought to be due to dynamic recrystallisation. The large variation in grain size for the thermally exposed specimen is a clear indicator of the inadequacy of the heat treatment employed. A stabilised grain size of 354 ± 48 μm was obtained after around 505h–540h at 650 °C, regardless of load applied.
- An increase in the number of carbides in the wrought alloy 718 during creep caused damage to accelerate in tertiary creep which results in a reduced creep life compared to LPBF alloy 718, despite having similar creep rates.
- The increase in precipitate density (δ phase, carbides or Laves) during creep is detrimental to the creep performance as it does not allow as much γ'' precipitation, which is the main strengthening mechanism for creep, and provides void initiation sites.
- During thermal exposure, pores expand and result in an increase in porosity. However, this is still less than the porosity caused by microvoids and damage during creep.
- The recommended microstructure for optimal creep performance includes large equiaxed grains, elimination of texture, dissolution of Laves and δ phase and the precipitation of small carbides and γ'' precipitates.

Future investigation on the effect of Kouraytem et al.'s recrystallisation heat treatment (625 °C/h ramp up rate, a 1 h dwell time at 1250 °C, and a 625 °C/h ramp down rate [76]), or a variant thereof, on the microstructure and creep performance of alloy 718 is recommended.

Author statement

- **Salomé Sanchez** – Methodology, Investigation, Analysis, Writing – original draft, writing - review & editing.
- **Gabriele Gaspard** – Investigation, Analysis.
- **Christopher J. Hyde** - Supervision, Writing - review & editing.
- **Ian A. Ashcroft** - Supervision, Writing - review & editing.
- **Adam T. Clare** – Supervision, Writing - review & editing.
- **Ravi Aswathanarayanaswamy** – Resources, Writing - review & editing.

Data availability

The raw/processed data required to reproduce these findings cannot be shared at this time due to technical or time limitations.

Declaration of competing interest

The authors declare that they have no known competing financial interests or personal relationships that could have appeared to influence the work reported in this paper.

Acknowledgments

This work has been supported by the Engineering and Physical Sciences Research Council [EP/S513854/1]. Thank you to Shane Maskill for grinding and creep testing the specimens and Alex Jackson-Crisp for machining the specimens.

References

[1] C.K. Chua, 3D printing and additive manufacturing : principles and applications (the 5th edition of Rapid prototyping : principles and applications), in: fifth ed., in: K.F. Leong (Ed.), Three Dimensional Printing and Additive Manufacturing, World Scientific, Singapore: Singapore, 2017. CheeKai Chua, Kah Fai Leong.
[2] B. Geddes, H. Leon, X. Huang, Superalloys : Alloying and Performance, ASM International, Materials Park, OH, 2010.
[3] A.R. Balachandramurthi, et al., Microstructural influence on fatigue crack propagation during high cycle fatigue testing of additively manufactured Alloy 718, Mater. Char. 149 (2019) 82–94.
[4] S. Sanchez, et al., Powder Bed Fusion of nickel-based superalloys: a review, Int. J. Mach. Tool Manufact. 165 (2021) 103729.
[5] L.N. Carter, Selective Laser Melting of nickel superalloys for high temperature applications, in: School of Metallurgy and Materials, University of Birmigham, Birmigham, 2013.
[6] Y.-L. Kuo, A. Kamigaichi, K. Kakehi, Characterization of Ni-based superalloy built by selective laser melting and electron beam melting, Metall. Mater. Trans. 49 (9) (2018) 3831–3837.
[7] Z. Xu, et al., Creep property of Inconel 718 superalloy produced by selective laser melting compared to forging, Mater. Sci. Eng., A 794 (2020) 139947.
[8] C. Hautfenne, S. Nardone, E. De Bruycker, Influence of heat treatments and build orientation on the creep strength of additive manufactured IN718, in: 4th International ECCC Conference, 2017 (Düsseldorf Germany.
[9] M. Pröbstle, et al., Superior creep strength of a nickel-based superalloy produced by selective laser melting, Mater. Sci. Eng., A 674 (2016) 299–307.
[10] Y.-L. Kuo, S. Horikawa, K. Kakehi, Effects of build direction and heat treatment on creep properties of Ni-base superalloy built up by additive manufacturing, Scripta Mater. 129 (2017) 74–78.
[11] T.D. McLouth, et al., Variations in ambient and elevated temperature mechanical behavior of IN718 manufactured by selective laser melting via process parameter control, Mater. Sci. Eng., A 780 (2020) 139184.
[12] S. Sanchez, et al., Multi-laser scan strategies for enhancing creep performance in LPBF, Additive Manufacturing 41 (2021) 101948.

[13] Z. Xu, et al., Creep behaviour of inconel 718 processed by laser powder bed fusion, J. Mater. Process. Technol. (2018) 256.
[14] F. Brenne, et al., Microstructural design of Ni-base alloys for high-temperature applications: impact of heat treatment on microstructure and mechanical properties after selective laser melting, Progress in Additive Manufacturing 1 (3) (2016) 141–151.
[15] Z. Xu, et al., Staged thermomechanical testing of nickel superalloys produced by selective laser melting, Mater. Des. 133 (2017) 520–527.
[16] S. Sanchez, et al., The creep behaviour of nickel alloy 718 manufactured by laser powder bed fusion, Mater. Des. 204 (2021) 109647.
[17] S. Azadian, Aspects of Precipitation in Alloy Inconel 718, Luleå tekniska universitet, 2004.
[18] S. Floreen, G.E. Fuchs, W.J. Yang, The metallurgy of alloy 625, Superalloys 718 (625) (1994) 13–37.
[19] M. Sundararaman, P. Mukhopadhyay, S. Banerjee, Carbide precipitation in nickel base superalloys 718 and 625 and their effect on mechanical properties, Superalloys 718 (1997) 625–706.
[20] W. Chen, M.C. Chaturvedi, Dependence of creep fracture of Inconel 718 on grain boundary precipitates, Acta Mater. 45 (7) (1997) 2735–2746.
[21] A.M. Mancisidor, et al., Reduction of the residual porosity in parts manufactured by selective laser melting using skywriting and high focus offset strategies, Phys. Procedia 83 (2016) 864–873.
[22] S. Sanchez, et al., Machine learning to determine the main factors affecting creep rates in laser powder bed fusion, J. Intell. Manuf. 32 (8) (2021) 2353–2373. https://doi.org/10.1007/s10845-021-01785-0.
[23] Q.Z. Chen, N. Jones, D.M. Knowles, The microstructures of base/modified RR2072 SX superalloys and their effects on creep properties at elevated temperatures, Acta Mater. 50 (5) (2002) 1095–1112.
[24] D. Deng, Additively manufactured inconel 718 : microstructures and mechanical properties, in: Linköping Studies in Science and Technology. Licentiate Thesis, Linköping University Electronic Press, Linköping, 2018, p. 69.
[25] W. Huang, et al., Heat treatment of Inconel 718 produced by selective laser melting: microstructure and mechanical properties, Mater. Sci. Eng. 750 (2019) 98–107.
[26] D. Kumar, et al., Texture dependent strain hardening in additively manufactured stainless steel 316L, Mater. Sci. Eng., A 820 (2021) 141483.
[27] G.E. Bean, et al., Build orientation effects on texture and mechanical properties of selective laser melting inconel 718, J. Mater. Eng. Perform. 28 (4) (2019) 1942–1949.
[28] M. Ni, et al., Anisotropic tensile behavior of in situ precipitation strengthened Inconel 718 fabricated by additive manufacturing, Mater. Sci. Eng., A 701 (2017) 344–351.
[29] O. Gokcekaya, et al., Unique crystallographic texture formation in Inconel 718 by laser powder bed fusion and its effect on mechanical anisotropy, Acta Mater. 212 (2021) 116876.
[30] L.H. Rettberg, T.M. Pollock, Localized recrystallization during creep in nickel-based superalloys GTD444 and René N5, Acta Mater. 73 (2014) 287–297.
[31] S.A.A. Shams, et al., Effect of grain size on the low-cycle fatigue behavior of carbon-containing high-entropy alloys, Mater. Sci. Eng., A 810 (2021) 140985.
[32] B. Song, et al., Vacuum heat treatment of iron parts produced by selective laser melting: microstructure, residual stress and tensile behavior, Mater. Des. 54 (2014) 727–733.
[33] L.C.M. Valle, et al., The effect of δ phase on the mechanical properties of an inconel 718 superalloy, J. Mater. Eng. Perform. 22 (5) (2013) 1512–1518.
[34] E.J. Mittemeijer, Fundamentals of Materials Science : the Microstructure-Property Relationship Using Metals as Model Systems/Eric J. Mittemeijer, Springer, London, 2010.
[35] F. Garofalo, Effect of grain size on the creep behavior of an austenitic lron - base alloy, Trans. AIME 230 (1964) 1460–1467.
[36] C. Berger, A. Thoma, A. Scholz, Creep modelling of waspaloy, in: PARSONS 2003: Sixth International Charles Parsons Turbine Conference, 2003.
[37] E. Loria, Superalloys 718, 625, 706 and Various Derivatives, 1994, p. 1994. Pittsburgh.
[38] E. Sadeghi, et al., Influence of thermal post treatments on microstructure and oxidation behavior of EB-PBF manufactured Alloy 718, Mater. Char. 150 (2019) 236–251.
[39] T. Vilaro, et al., Microstructural and mechanical approaches of the selective laser melting process applied to a nickel-base superalloy, Mater. Sci. Eng., A 534 (2012) 446–451.
[40] K. Chen, J. Dong, Z. Yao, Creep Failure and Damage Mechanism of Inconel 718 Alloy at 800–900 °C, Metals and Materials International, 2019.
[41] L.Y. Wang, et al., Small punch creep performance of heterogeneous microstructure dominated Inconel 718 fabricated by selective laser melting, Mater. Des. (2020) 195.
[42] M. Jouiad, et al., Microstructure and mechanical properties evolutions of alloy 718 during isothermal and thermal cycling over-aging, Mater. Des. 102 (2016) 284–296.
[43] R.C. Reed, in: R.C. Reed (Ed.), The Superalloys: Fundamentals and Applications, Cambridge University Press, Cambridge (UK), 2006.
[44] M. Kaufman, A. Palty, The phase structure of Inconel-718 and Inconel-702 alloys, Transactions of the metallurgical society of AIME 221 (6) (1961) 1253–1262.
[45] S. Goel, et al., Microstructure evolution-based design of thermal post-treatments for EBM-built Alloy 718, J. Mater. Sci. 56 (8) (2021) 5250–5268.
[46] T. Gundgire, et al., Response of different electron beam melting produced Alloy 718 microstructures to thermal post-treatments, Mater. Char. 167 (2020) 110498.
[47] J.M. Poole, K.R. Stultz, J.M. Manning, The Effect of INGOT Homogenization Practice on the Properties of Wrought Alloy 718 and Structure, Superalloys, 1989, pp. 219–228.
[48] J. Brooks, P. Bridges, Metallurgical stability of Inconel alloy 718, Superalloys 88 (1988) 33–42.
[49] A. Mitchell, et al., The precipitation of primary carbides in alloy 718, superalloys 718 (625,706) (1994) 65–78.
[50] R. Eriksson, J. Moverare, Z. Chen, A low cycle fatigue life model for a shot peened gas turbine disc alloy, Int. J. Fatig. 124 (2019) 34–41.
[51] C.T. Sims, N.S. Stoloff, W.C. Hagel, Superalloys II, vol. 8, Wiley, New York, 1987.
[52] R.W. Hayes, Creep Deformation of Inconel alloy 718 in the 650°C to 760°C temperature regime, in: E.A. Lorin (Ed.), Superalloys 718, 625 and Various Derivatives, Northridge, California, 1991.
[53] X.S. Xie, et al., The precipitation strengthening effect of Nb, Ti and Al in cast/wrought Ni-base superalloys, in: Materials Science Forum, Trans Tech Publ, 2010.
[54] C.M. Kuo, et al., Aging effects on the microstructure and creep behavior of Inconel 718 superalloy, Mater. Sci. Eng., A 510–511 (2009) 289–294.
[55] Y.-C. Lin, et al., Hot tensile deformation behaviors and fracture characteristics of a typical Ni-based superalloy, Mater. Des. 55 (2014) 949–957.
[56] Y. Huang, T.G. Langdon, The evolution of delta-phase in a superplastic Inconel 718 alloy, J. Mater. Sci. 42 (2) (2007) 421–427.
[57] B. Hassan, J. Corney, Grain boundary precipitation in Inconel 718 and ATI 718 Plus, Mater. Sci. Technol. 33 (16) (2017) 1879–1889.
[58] H. Zhang, et al., Delta precipitation in wrought Inconel 718 alloy; the role of dynamic recrystallization, Mater. Char. 133 (2017) 138–145.
[59] ASTM International, F3055-14a Standard Specification for Additive Manufacturing Nickel Alloy (UNS N07718) with Powder Bed Fusion, 2014. West Conshohocken, PA.
[60] SAE International, Heat treatment wrought nickel alloy and cobalt alloy parts, SAE International (2001).
[61] S. Goel, et al., Microstructure evolution and mechanical response-based shortening of thermal post-treatment for electron beam melting (EBM) produced Alloy 718, Mater. Sci. Eng., A 820 (2021) 141515.
[62] G. Marchese, et al., Microstructural evolution of post-processed Hastelloy X alloy fabricated by laser powder bed fusion, Materials 12 (3) (2019).
[63] M. Ahmad, et al., Structure, texture and phases in 3D printed IN718 alloy subjected to homogenization and HIP treatments, Metals 7 (6) (2017) 196.
[64] A. Balachandramurthi, et al., Additive manufacturing of alloy 718 via electron beam melting: effect of post-treatment on the microstructure and the mechanical properties, Materials 12 (1) (2018) 68.
[65] D. Tomus, et al., Influence of post heat treatments on anisotropy of mechanical behaviour and microstructure of Hastelloy-X parts produced by selective laser melting, Mater. Sci. Eng., A 667 (2016) 42–53.
[66] K. Moussaoui, et al., Effects of Selective Laser Melting additive manufacturing parameters of Inconel 718 on porosity, microstructure and mechanical properties, Mater. Sci. Eng., A 735 (2018) 182–190.
[67] S. Sui, et al., Investigation of dissolution behavior of laves phase in inconel 718 fabricated by laser directed energy deposition, Additive Manufacturing 32 (2020) 101055.
[68] S. Sui, et al., The influence of Laves phases on the room temperature tensile properties of Inconel 718 fabricated by powder feeding laser additive manufacturing, Acta Mater. 164 (2019) 413–427.
[69] H. Xiao, et al., Laves phase control of Inconel 718 alloy using quasi-continuous-wave laser additive manufacturing, Mater. Des. 122 (2017) 330–339.
[70] W.M. Tucho, et al., Microstructure and hardness studies of Inconel 718 manufactured by selective laser melting before and after solution heat treatment, Mater. Sci. Eng., A 689 (2017) 220–232.
[71] E. Bassini, G. Marchese, A. Aversa, Tailoring of the microstructure of laser powder bed fused inconel 718 using solution annealing and aging treatments, Metals 11 (6) (2021).
[72] L. Geng, Y.-S. Na, N.-K. Park, Continuous cooling transformation behavior of Alloy 718, Mater. Lett. 30 (5) (1997) 401–405.
[73] T.G. Gallmeyer, et al., Knowledge of process-structure-property relationships to engineer better heat treatments for laser powder bed fusion additive manufactured Inconel 718, Additive Manufacturing 31 (2020) 100977.
[74] R. Jiang, et al., Effect of Heat Treatment on Microstructural Evolution and Hardness Homogeneity in Laser Powder Bed Fusion of Alloy 718, Additive Manufacturing, 2020, p. 35.
[75] E. Chlebus, et al., Effect of heat treatment on the microstructure and mechanical properties of Inconel 718 processed by selective laser melting, Mater. Sci. Eng., A 639 (2015) 647–655.
[76] N. Kouraytem, et al., A recrystallization heat-treatment to reduce deformation anisotropy of additively manufactured Inconel 718, Mater. Des. 198 (2021) 109228.
[77] Y. Zhao, et al., A new high-throughput method using additive manufacturing for alloy design and heat treatment optimization, Materialia 13 (2020) 100835.